RSC Advances

ROYAL SOCIETY OF CHEMISTRY

www.rsc.org/advances

Journal Name

RSCPublishing

ARTICLE

High sulfur loaded carbon aerogel cathode for lithium-sulfur batteries

Cite this: DOI: 10.1039/x0xx00000x

K. Balakumar and N. Kalaiselvi*

Abstract: An attempt made to improve sulfur loading in a template free porous carbon to the extent of 70 wt. % has inferred two interesting observations, viz., 60 wt. % sulfur loading exhibits superior electrochemical properties in the S@C composite form and an enhanced 73 wt. % sulfur loading leads to the formation-cum-stabilisation of sulfur in its monoclinic phase. Carbon aerogel with tunable properties, derived from the catalyst aided cross linking of resorcinol and formaldehyde, possessing a specific surface area of 1395 m^2/g and pore volume of 1.423 cm^3/g has been exploited for sulfur loading to form series of S@C composites. Interestingly, carbon aerogel prepared in the present study offers multifarious advantages such as conducting additive, potential host to accommodate higher concentration of sulfur and better polysulfide confining matrix. The 60 wt. % sulfur loaded carbon aerogel composite exhibits an appreciable specific capacity of 600 mAh/g at C/10 rate up to 100 cycles, 480 mAh/g at 1C and 422 mAh/g at 2C rate. Hence, the capability of carbon aerogel, synthesized through the present study in accommodating higher concentration of sulfur, effective management of polysulfide shuttle and provision of favorable electrode-electrolyte interface to facilitate extended cycling possibilities at different current densities has been demonstrated.

Received 00th January 2012,
Accepted 00th January 2012

DOI: 10.1039/x0xx00000x

www.rsc.org/

1. Introduction

The ever increasing energy demands, depleting fossil fuels and the need for greener and cleaner environment force the direction of research on renewable energy and energy storage systems as an impeccable choice. In this regard, lithium–ion battery could be considered as a superior storage system for hybrid electric vehicles by its light weight, high operating voltage and high theoretical capacity than other secondary batteries.[1-2] However, to meet with the required energy density for hybrid electric vehicle applications, lithium-ion batteries pose problems arising from the inferior theoretical capacity of heavier transition metal (Fe, Co) based cathodes in stabilizing the structure and the number of electrons transferred corresponding to the intercalation and de-intercalation of lithium ions.[3-5] Interestingly, lithium-sulfur system circumvents these issues with the general aspects of low cost, environmentally benign and abundant nature of sulfur, which is used as a cathode. Considering the transfer of two electrons per sulfur, the theoretical capacity of 1675 mAh/g and the high theoretical energy density of 2600 Wh/Kg of lithium-sulfur battery could be understood based on the simplified over all reaction[6-7]

$$16Li + S_8 \longleftrightarrow 8Li_2S$$

However, the incredible performance of lithium-sulfur system is hindered by factors such as insulating nature of sulfur ($5x10^{-30}$ S cm^{-1} at 25°C), electrochemically generated solid/soluble reaction products, shuttling reaction between long and small chain polysulfides, irreversible deposition of Li_2S and/or Li_2S_2, unavoidable volume changes of the cell upon cycling and the storage performance of sulfur.[8-10] So, sulfur should be embedded in an electrically conductive, polysulfide confining matrix that may buffer the volume changes associated with the Li-S system. Towards this direction, engineering of electrodes with required pore size, pore volume and surface area to ensure better utilization of sulfur in the electrochemical cell assembly is the potential approach to qualify lithium-sulfur batteries for practical applications.

Solution mediated infiltration of sulfur into activated mesoporous carbon[10], confinement of sulfur in ordered porous carbon by melt diffusion strategy with polymer coating[11], infusion of sulfur into hollow carbon to ensure untroubled charge transport even at high rated current and effective trapping of polysulfides[12], hollow carbon fiber host for sulfur guest in a small wall thickness of carbon for beneficial electron and lithium ion movement[13], superior performance of graphite plane intercalated sulfur in disordered carbon[14] are the few examples of carbon based sulfur electrodes that demonstrate the superiority and suitability of the same for application in Li-S batteries.

In addition to carbon, graphene-sulfur[15] and carbon black attached graphene wrapped PEG covered sulfur[16] to increase the utility of sulfur are reported in the literature. Graphene with several unique properties[17], despite being considered as a beneficial additive for lithium-ion batteries at high rate applications[18], could not solve the issues of sulfur cathode[15] and it requires specific structures to ensure high utilization of sulfur.[16] Further, conducting polymers such as polypyrrole[19], polythiophene[20], poly(3,4-ethylenedioxy-thiophene)[21], polyaniline[22] and poly(acrylonitrile)[23] have also been deployed to chemically and/or physically confine sulfur and polysulfides to alleviate the undesired dissolution, apart from enhancing the conductivity to improve the overall performance of Li-S batteries. Similarly, polysulfide adsorbing insulating materials such as SiO_2 and Al_2O_3 are also reported to improve the electrochemical performance of sulfur cathode in Li-S system.[25-26]

Among the existing cathodes, carbon based sulfur composites are preferred, due to the provision of facile electron channel to sulfur and better polysulfide confinement. Mostly, such porous carbon materials for sulfur are obtained by means of template methods, which involve number of sequences and hence tedious. On the other hand, the present study deals with the development of carbon aerogel, wherein porous nature has been achieved by cross-linking during sol-gel condensation, thus excluding porogen elimination. Such an aerogel assumes importance for its ability to tailor the pores and morphology, by tuning the synthesis conditions and accordingly the impregnation and utilization efficiency of loaded sulfur could also be modified. Herein, acid catalysed cross linkage formation and the deployment of optimized pH[27-28] are taken in to special consideration to obtain the carbon aerogel with large surface area, desired pore size, distribution of pores and pore volume. Because, it is well known that while microporous carbon facilitates higher rate performance of sulfur cathode, the mesoporous carbon enhances lithium transport properties, besides ensuring the confinement of polysulfides and sulfide ions obtained from the electrochemical reaction. In other words, microporous carbon suffers from lower sulfur loading and the mesoporous nature enhances the rate capability behavior of sulfur cathode. Further, it is well known that the amount of loaded and utilized sulfur in the cathode determines the volumetric energy density of the cell.[28]

Based on these grounds, mesoporous carbon aerogel from acid mediated resorcinol-formaldehyde (RF) sol-gel reaction, obtained at a pH of below 6 has been prepared with a specific surface of 1395 m^2/g, which is found to be bestowed with the possibility of accommodating higher amount of sulfur. The currently prepared carbon aerogel containing 60 wt. % sulfur supersedes the previous work with limited volumetric energy density.[29] The appreciable performance of S@C composites containing different concentrations of sulfur loading has been demonstrated. Higher sulfur loading and the maintenance of appreciable capacity of 600 mAh/g upon extended cycling (up to 100 cycles) are the twin advantages achieved from the currently developed sulfur cathode, impregnated in a carbon aerogel, consisting of mesoporous carbon in larger proportion along with the co-existence of micropores.

2. Experimental Section

2.1. Materials

All the chemicals were obtained from Sigma-Aldrich/ Alfa Aesar. Deionized water with a conductivity of 0.055 μS/cm has been used. All the chemicals were used without any further purification.

2.2. Synthesis of SCAC

Resorcinol-formaldehyde (RF) gel was obtained using R:F =1:2 and R:C=50:1. For R:F= 1:2, the typical mole ratio corresponds to 0.29 M of R and 0.58 M of F. The precursor was dissolved in deionized water with stirring and the pH of the solution was brought below 6 by the careful addition of dilute nitric acid, without changing the temperature of the solution. The solid content of the solution was maintained as 50 wt. %. After stirring for half an hour, the solution was transferred to a hydrothermal setup and maintained at 85 °C for a week. The obtained deep red gel was washed well with deionized water to remove the residual catalyst and kept in acetone bath at 50 °C for 3 days for water replacement. The water replaced gel was dried at 50 °C for 1 day and carbonized at 800 °C over a period of 3 h at a ramp rate of 1.5 °C/min. The product thus obtained contains 40 % RF by weight and it is designated as CA. Sulfur-carbon aerogel composites (designated as SCAC-X where X= 40, 50, 60, 66, 73 wt. % of sulfur) have been obtained by melt diffusion strategy. Required amount of sulfur was mixed well with CA and kept at 280 °C for 12 h to obtain SCAC-X composites. Subsequently, the product was cooled down to room temperature at a cooling rate of 2 °C/min.

2.3. Electrode Fabrication and Coin Cell Assembly

To prepare the electrode, the sulfur-carbon aerogel composite (SCAC-X) was mixed with super-P carbon black and polyvinylidene fluoride binder in the weight ratio of 80:10:10 and N-methyl-2- pyrrolidone was used to obtain a slurry. This slurry was coated over aluminium foil current collector and then dried at 60 °C for 12 h. The electrochemical performance of SCAC-X has been studied using 2032 coin cells (Hohsen Corporation) by deploying the electrode punched out from the coated foil with a diameter of 15.9 mm as working electrode. Lithium metal was used as counter and reference electrode and polypropylene separator has been used. The electrolyte used was 1M lithium bis(trifluoromethanesulfonyl)imide and 0.1M lithium nitrate, dissolved in a co-solvent of 1,3-dioxolane and 1,2-dimethoxyethane (1:1v/v ratio).

2.4. Characterization

The prepared CA and sulfur-carbon aerogel composites (SCAC-X) were analysed using the following instruments. XRD was recorded with the Bruker D8 Advance X-ray diffractometer (XRD) using Ni-filtered Cu Kα radiation. TGA and Raman spectral studies of SCAC-X were performed using TA Instruments SDT Q600 thermogravimetric analyzer and Renishaw Invia Raman Microscope using He-Ne LASER at an exciting wavelength of 633 nm respectively. N_2 adsorption/desorption isotherm was obtained from Quantachrome Instruments version 11.02 and XPS results from MULTILAB 2000 Base system. Morphology changes after sulfur loading and elemental mapping were studied using Gemini Field Emission Scanning Electron Microscopy (FESEM), Tecnai 20 G2 (FEI make) Transmission Electron Microscopy (TEM) and STEM JEOL, JEM 2100 respectively. Cyclic Voltammetry (CV) and impedance measurements were carried out using a VMP3 multichannel potentiostat–galvanostat system (Biologic Science Instrument). Charge–discharge studies were carried out using Arbin charge–discharge cycler.

3. Results and Discussion

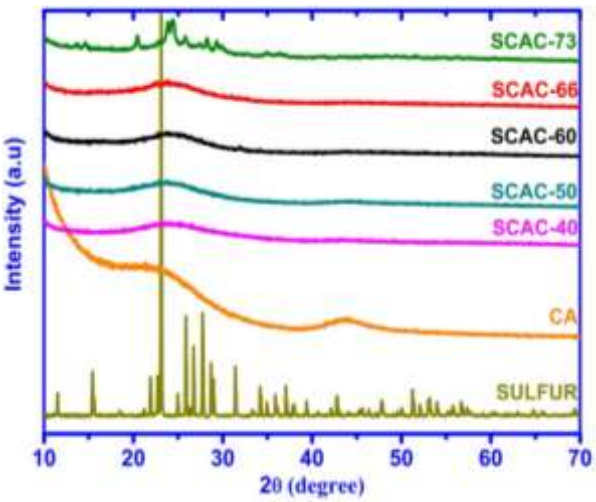

Fig. 1 XRD pattern of sulfur, carbon aerogel, 40 wt. %(SCAC-40), 50 wt. %(SCAC-50), 60 wt. %(SCAC-60), 66 wt. %(SCAC-66) and 73 wt. %(SCAC-73) sulfur loaded carbon aerogel.

XRD pattern of sulfur, carbon aerogel and the series of SCAC composites is shown in Fig. 1. Herein, CA exhibits two broad peaks around 2θ=24 and 44°, corresponding to the (002) and (101) graphite planes, thus indicating the amorphous nature of carbon. The d-spacing value calculated for (002) plane is 0.370 nm. Crystalline peaks of sulfur indicate the *fddd* orthorhombic structure, which are matching with the JCPDS pattern No: 08-0248. From the XRD pattern of composites, it is clear that the melt diffused crystalline sulfur has been converted to the amorphous state. Further, it provides an indication that more likely the molten sulfur diffuses into the porous structure of carbon aerogel, where it gets solidified and the structural growth upon heat treatment and consequent cooling is limited to the pores size of the carbon aerogel. The decrease in intensity of broad carbon peak indicates the presence of sulfur in a well dispersed state. Interestingly, the absence of crystalline peaks corresponding to sulfur in CA (from SCAC-40 to SCAC-66) indicates that CA can accommodate sulfur upto 66 wt. % in the available pores (more discussion is available under N_2 isotherm section). On the other hand, the solidification of sulfur shows distinct and peculiar behavior for higher amount (>66 wt. %) of loading. In other words, the appearance of less intense crystalline peaks of SCAC-73 matches with the monoclinic system (JCPDS No: 79-1517) rather than the orthorhombic structure, thus evidencing the fact the carbon aerogel stabilizes sulfur in its monoclinic phase at room temperature, especially when the loading concentration exceeds 66 wt. %, which is in line with a similar report on carbon nanotube[30]. i.e., 73 wt. % of sulfur content is slightly higher than the maximum possible level of loading with respect to the currently prepared carbon aerogel. Hence, one can understand that the carbon aerogel of the present study can accommodate a sulfur content as high as ~70 wt. %, which is an interesting observation.

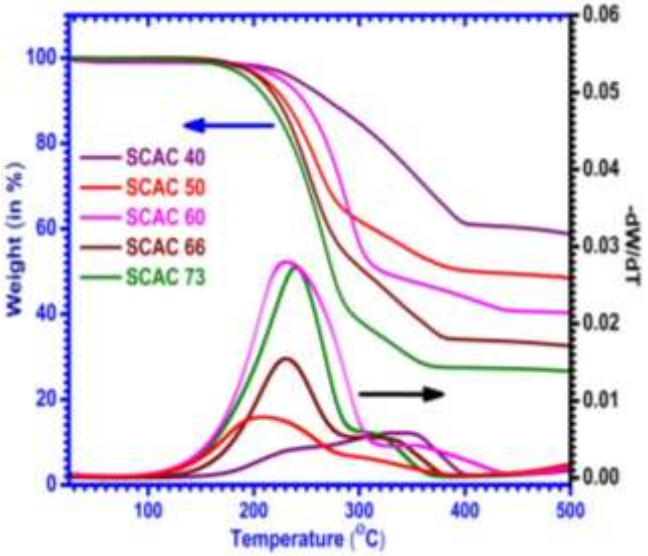

Fig. 2 Thermogravimetry analysis of sulfur-carbon aerogel composites.

Thermogravimetry analysis was performed under nitrogen atmosphere and upto 500 °C with a heating rate of 10 °C/ min. From this measurement, -dW/dT versus temperature has been plotted and is displayed in Fig. 2 along with the variation in weight loss as a function of temperature. The amount of sulfur in CA has been calculated based on the weight loss of the composite at 500° C and these values are used to formulate and denote the samples with a general representation SCAC-X, where X stands for the sulfur content (e.g. SCAC-40 contains 40 wt. % of sulfur). In other words, the adsorption ability of carbon aerogel for various amounts of sulfur loading can be evaluated using TGA analysis. Since it is based on the evaporation of sulfur from the pores of carbon aerogel, the

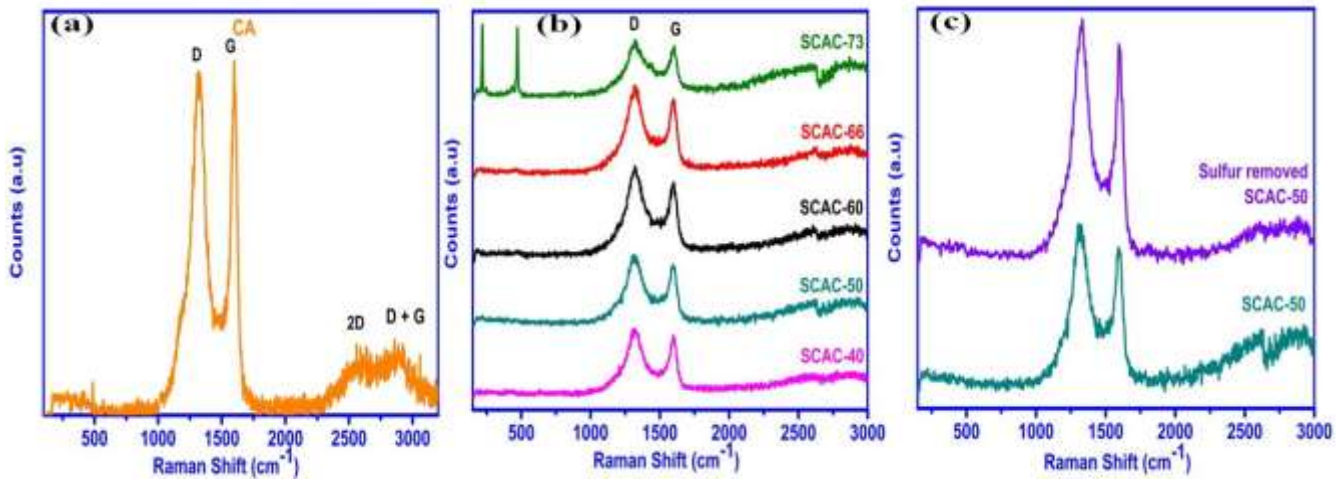

Fig. 3 Raman spectrum of (a) carbon aerogel, (b) sulfur-carbon aerogel composites and (c) 50 wt. % sulfur loaded and sulfur removed carbon aerogel composites.

region occupied by –dW/dT versus temperature curve indicates the adsorption ability of CA vs. amount of sulfur loading.[10] From Fig. 2, it is evident that major weight loss occurs at 240° C for SCAC-60 that occupies the highest region than other SCAC samples, thus inferring the need for more thermal energy to remove sulfur from CA. Hence, the relatively superior thermal stability of SCAC-60 composite could be understood.

	D-Raman shift (cm^{-1})	G-Raman shift (cm^{-1})	I_D	I_G	I_D/I_G	L_a (nm)
CA	**1320.23**	**1597.91**	**510.96**	**526.40**	**0.97**	**39.45**
SCAC-40	**1315.58**	**1597.03**	**333.07**	**302.00**	**1.10**	**34.72**
SCAC-50	**1319.30**	**1601.46**	**312.45**	**266.58**	**1.17**	**32.67**
SCAC-60	**1321.16**	**1597.91**	**464.12**	**386.24**	**1.20**	**31.86**
SCAC-66	**1316.51**	**1597.03**	**453.23**	**388.39**	**1.17**	**32.81**
SCAC-73	**1325.85**	**1604.12**	**298.73**	**271.16**	**1.10**	**34.76**

Table 1 Crystallite size and other parameters derived from Raman spectral behavior of carbon aerogel and S@C composite.

Raman microscopy is a non-destructive technique, which is a powerful tool to analyse the nature of carbon materials such as graphitic or amorphous. It is quite reasonable to study the change in the structure of carbon in the carbon aerogel, especially upon sulfur loading and its interaction using this technique. In Fig. 3(a), the intense in-plane stretching vibration of pairs of sp^2 carbon corresponding to E_{2g} symmetry (G band) that appears at 1597 cm^{-1}, defect or graphite stimulated six fold aromatic ring breathing vibration corresponding to A_{1g} (D band) at 1320 cm^{-1} along with the overtone of in-plane phonon related 2D peak centered at ~ 2581 cm^{-1} and D+G peak at ~ 2896 cm^{-1} are evident. The presence of such a combination of D, G, 2D and D+G peaks confirms the presence of nano and polycrystalline graphitic carbon tied with amorphous carbon in the currently prepared carbon aerogel.[31] The crystallite size L_a[32] can be calculated from the intensity ratio of D and G bands, which is about 39.45 nm.

Raman spectra of chosen combination of sulfur-carbon aerogel composites are shown in Fig. 3(b). It is quite interesting to note that the I_D/I_G ratio increases upon sulfur loading (Table 1), as evident from the increasing intensity of broader D band that surpasses the narrow G band. However, the I_D/I_G value increases from SCAC-40 to SCAC-60 and decreases thereafter with the increasing concentration of sulfur (such as SCAC-66 and SCAC-73). Hence, it is understood that the amount of sulfur dispersed into the carbon aerogel could be quantified using the calculated I_D/I_G values i.e., with the increasing loading of sulfur, disorder also increases in the carbon aerogel with an exception of SCAC-66 and SCAC-73. However, Raman spectrum recorded for SCAC-73 is entirely different from the rest of the composites, as it contains the co-existing Raman signatory peaks due to sulphur and CA. This in turn is an indication that a small portion of sulfur remains on the surface of the CA, besides filling the pores of carbon aerogel. From this observation, it is understood that a concentration of 73 wt. % sulfur is slightly excess than the maximum possible concentration that could be accommodated in the pores of the CA, thus helping us to conclude that nearly 70 wt. % sulfur uptake is possible with the currently prepared CA that blocks the surface of CA partially. This is in agreement with the XRD results, wherein peaks corresponding to CA are not visible in SCAC-73. The effect of sulfur loading in changing the graphitic nature of CA towards amorphous form is well understood from

the comparison of Raman spectra in Fig. 3(c) of SCAC-50 and the corresponding sulfur removed CA (sulfur has been removed by heating SCAC-50 in N_2 atmosphere for 2h at 500 °C and the temperature has been fixed based on TGA study). Such a typical and random analysis of Raman spectral behavior confirms the fact that the added sulfur plays a vital role in changing the slightly pronounced amorphous nature of CA gradually. However, the co-existence of graphitic and amorphous nature of CA is always beneficial for sulfur cathode in terms of electrical network (otherwise known as carbon wiring) and buffers the volume changes. Hence, Raman study offers an indication that SCAC-60 may give rise to better electrochemical behavior compared with the rest of the composites and SCAC-73 composite may not be suitable for application in Li-S batteries (as inferred from XRD also).

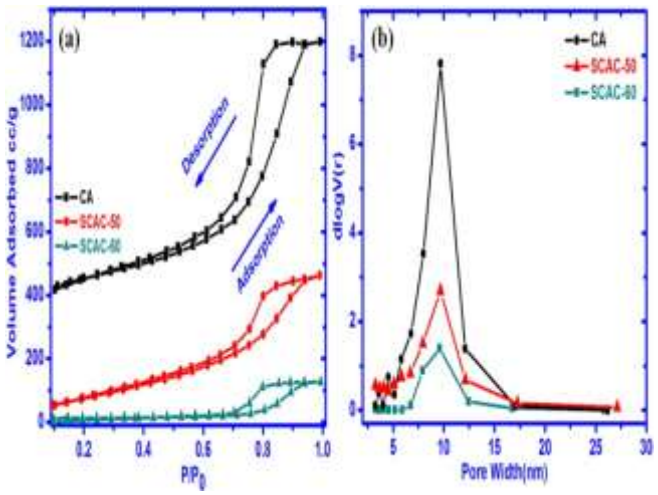

Fig. 4 (a) Nitrogen adsorption-desorption isotherm of carbon aerogel and select sulfur-carbon aerogel composites and (b) corresponding pore volume distribution.

Nitrogen adsorption-desorption isotherms were recorded at 77 K for the CA, SCAC-50 and SCAC-60 in the range of relative pressure P/P_0 from 0.1 to 1.0. The isotherm curve in Fig. 4(a) corresponding to carbon aerogel exhibits type-IV isotherm with H1 hysteresis[33] and the capillary condensation is centered at a relative pressure of 0.82. Similar behavior has been noticed for SCAC-50 and SCAC-60, except the decrease in adsorbed volume observed as a function of increasing sulfur content. The decrease in adsorbed volume is an evidence that the elemental sulfur occupies the available pores of CA. BET surface area and related parameters of CA are calculated and the values of surface area, maximum pore width and pore volume are tabulated (Table 2). Surprisingly, higher specific surface area and pore volume of 1395 m^2/g and 1.423 cm^3/g have been calculated for CA, corresponding to a maximum width of 9.676 nm of carbon aerogel, deduced from the pore distribution curve (Fig. 4(b)). It is quite reasonable and impetus to use such a carbon aerogel with an appreciable high surface area to impregnate sulfur and to exploit the same as a potential cathode for Li-S system. Such an idea gets validated based on the highest theoretical loading possibility of sulfur, which has been calculated to be 74.66% in CA. As expected, the pore volume and surface area of CA decrease with the increasing sulfur loading, thus substantiating the assumption that the probable location of sulfur is in the pores. For 50 wt. % loading, the specific pore volume and specific surface area are reduced to 0.707 cm^3/g and 331.046 m^2/g and for 60 wt. % loading, it further reduces to 0.237 cm^3/g and 16.830 m^2/g respectively. These values are consistent with the previous inference related to the location of sulfur in CA host at the pores. As a result, enhanced electrical conductivity and better buffering to admit the volume expansion during cycling performance are expected with the currently designed sulfur impregnated carbon aerogel.

Sample	Pore Radius (nm)	Specific surface Area (m^2/g)	Specific Pore Volume (cm3/g)
CA	9.68	1395.62	1.42
SCAC-50	9.63	331.05	0.71
SCAC-60	9.60	16.83	0.24

Table 2 Textural parameter of carbon aerogel and select concentration of sulfur loaded carbon aerogel.

FESEM images of carbon aerogel at low and high magnification are shown in Fig. 5(a) and (b). It is obvious from the figure that the particles are properly interconnected with each other to enable three dimensional electron conduction and the particle size is found to be less than 100 nm. The available pores of the interconnected particles render transport path to sulfur, especially during the melt diffusion and aided the confinement of sulfur in the porous structure. TEM image in Fig. 5(c) also shows the interconnected network of CA, wherein region that appears as grey corresponds to the overlap at the edges. However, three or more particles also overlap at the corners and give rise to slightly dark regions, wherein the increased thickness is responsible for the observed darkness. Further, the amorphous nature of the carbon aerogel is understood from the corresponding SAED pattern appended as an inset of Fig. 5(c). In contrast to Fig. 5(c), HRTEM image of SCAC-60 in Fig. 5(d) contains periodically varying grey and black colour patterns. Not obvious any overlap of two or more particles in the black area and hence the black colour region is believed to be due to the presence of impregnated sulfur while the grey region corresponds to that of carbon aerogel. The appearance of periodic pattern of black and grey area is due to the homogeneous distribution of embedded sulfur into the pores of carbon aerogel, thus evidencing the effective and uniform confinement of sulfur in CA. The corresponding SAED pattern in the inset of Fig. 5(d) confirms the amorphous nature of sulfur impregnated in the carbon aerogel and the same has been substantiated by the XRD results of S@C composites. TEM lattice fringes with a spacing of 0.365 nm (Fig. 5(e)) coincide with the d-spacing in XRD pattern of CA($d_{(002)}$=0.370 nm), thus

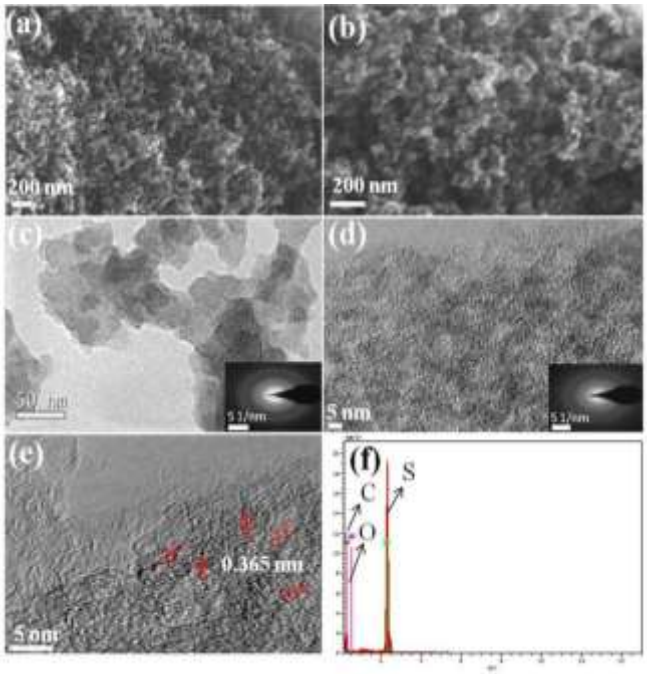

Fig. 5 (a) Low and (b) high magnification FESEM images of carbon aerogel (c) TEM image (inset-SEAD pattern) of carbon aerogel (d) Low and (e) high magnification HRTEM images (inset-SEAD pattern) and (f) EDX spectrum of 60 wt. % of sulfur loaded carbon aerogel.

validating the correlation of TEM based results with those of XRD. The discontinued lattice fringe patterns observed throughout the TEM image confirms the co-existence of disordered and graphitic nature of CA, which coincides with the results of Raman studies. Energy dispersive X-ray spectrum of SCAC-60 (Fig. 5(f)) shows pronounced peaks for carbon and sulfur and negligibly small signature for oxygen, thus confirming the elemental composition and stoichiometry of the title cathode with an unavoidable association of trace amount of oxygen (which is not unusual).

In order to confirm the uniform distribution of sulfur in the carbon aerogel, elemental mapping has been done by scanning transmission electron spectroscopy (STEM) for SCAC-60 sample. The area selected for mapping is shown in Fig. 6(a). STEM mapping suggests that sulfur is uniformly distributed in the carbon aerogel and the cumulative mapping results in Fig. 6(d) further ensures the intimate contact of sulfur with the carbon aerogel.

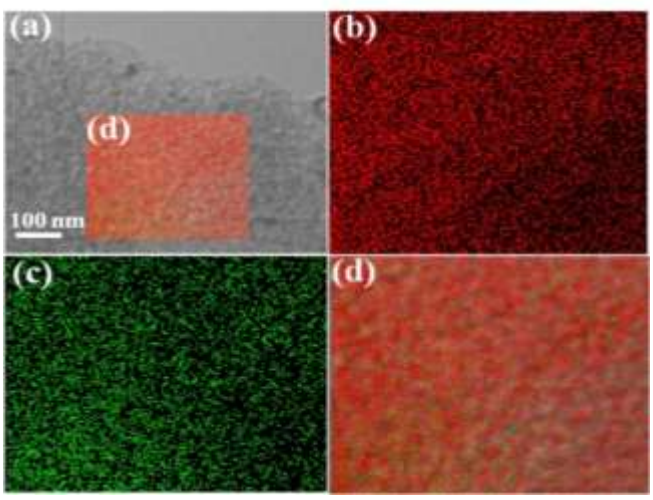

Fig. 6 (a) Selected area of SCAC-60 composite subjected to elemental mapping (b) carbon (c) sulfur and (d) cumulative carbon elemental mapping image.

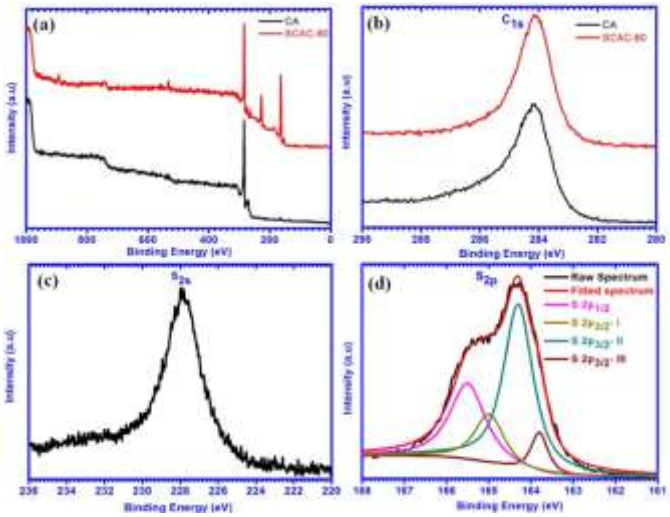

Fig. 7 (a) Survey spectra, (b) 1s carbon spectra of CA and SCAC-60 and (c) and (d) correspond to 2s and 2p spectra containing fitted photoelectron lines of sulfur in SCAC-60 respectively.

The elements present and the corresponding oxidation state of loaded sulfur in CA can be identified using XPS analysis, which in turn could be used to substantiate the observations made from Raman studies. Fig. 7(a) shows survey spectra of CA and SCAC-60 and the individual scans of identified peaks are shown in Fig. 7(b)-(d). Carbon and elemental oxygen are identified in CA and carbon, sulfur and oxygen are present in SCAC-60 as per Fig 7(a). The oxygen found in the XPS analysis may be an adsorbed atmospheric oxygen in CA. The peak appeared at 284.14 and 284.17 eV for CA and SCAC-60 in Fig 7(b) reveals that the binding energy of 1s electron of the C-C bond[34] in carbon aerogel, corresponding to the full width at half maximum (FWHM) of CA is 1.43 eV, while it is 1.73 eV for SCAC-60. Sulfur 2s peak appeared at 222.80 eV (Fig. 7(c)) and the 2p peaks of sulfur contain more information about the bonding nature of sulfur in carbon aerogel. As presented in Fig. 7(d), the 2p raw spectrum of sulfur can be deconvoluted into four component peaks. The peak at 165.50 eV corresponds to $2p_{1/2}$ spin-orbital coupling of 2p electrons and the other peak ($2p_{3/2}$-I, $2p_{3/2}$-II and $2p_{3/2}$-III) values at 165.0, 164.30 and 163.80 eV correspond to the presence of S═O, $2p_{3/2}$ spin-orbital coupling and C─S bond respectively.[35-36] Hence, it is confirmed from XPS analysis that some of the sulfur atoms are chemically bonded to the carbon aerogel.

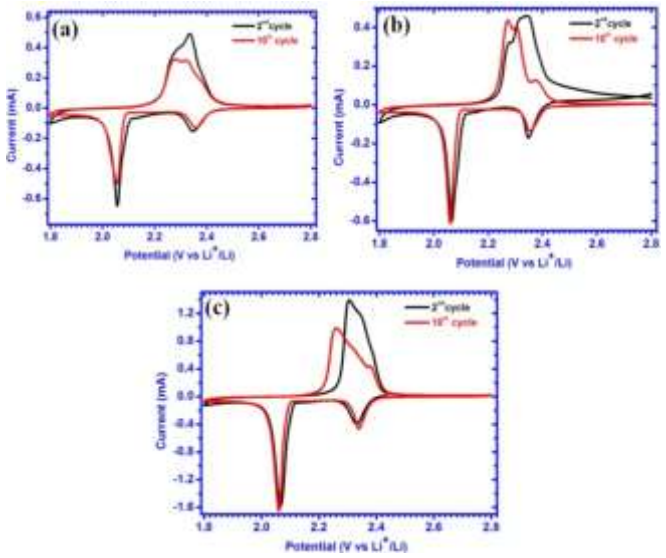

Fig. 8 Second and tenth CV cycle behavior of (a) SCAC-50 (b) SCAC-60 and (c) SCAC-66 composite cathode recorded at a scan rate of 0.1 mV/s

Cyclic voltammetry behavior of 50 (Fig. 8(a)), 60 (Fig 8(b)) and 66 (Fig. 8(c)) wt. % sulfur loaded CA cathodes shows typical and characteristic peaks of sulfur with a slight difference between initial and progressive CV cycles. Two sharp and distinguishable cathodic peaks are observed, which evidence the disproportional electrochemical reduction of elemental sulfur into higher order polysulfides and their subsequent cathode reduction to Li_2S/Li_2S_2 upon extended cathodic potential. The first reduction peak appears at a potential of 2.35, 2.35 and 2.33 V corresponding to SCAC-50, 60, 66 cathodes during the initial cycle and the same is shifted respectively to 2.36, 2.35 and 2.34 V upon progressive cycling (10^{th} CV cycle). The shift in potential upon progressive cycling is found to be admissibly small for SCAC-50 and SCAC-60 cathodes, while the difference in SCAC-66 cathode is little significant. The utilization of sulfur is found to be higher only upon progressive cycling with a special reference to SCAC-66 cathode, which is an indication that the initial volume expansion of sulfur in carbon aerogel hampers the complete utilization of active material. Second reduction peak potential of SCAC-(50, 60, and 66) cathodes appears at 2.06, 2.07 and 2.07 V and 2.06, 2.06 and 2.06 V corresponding to the 2^{nd} and 10^{th} cycle respectively. No obvious change in peak potential has been noticed for all the three chosen concentration of sulfur. However, the peak current value is found to get reduced upon extended cycling with an exception of SCAC-60 cathode. In other words, more surface area of SCAC-50 cathode active material that gets exposed to the electrolyte available in unfilled pores enhances the dissolution of active material.[37]

Subsequent anodic scan exhibits one broader peak for single step conversion of Li_2S_2/Li_2S into Li_2S_8/S_8. But the CV peak pattern pertinent to the initial and extended cycles is entirely different. Moving from SCAC-50 to 66, the anodic peaks shift towards the cathodic direction and SCAC-50 shows exact confinement of 10^{th} cycle with that of the 2^{nd} cycle, except the reduced overall current that slightly shifts the peak current position at 2.38 V. On the other hand, SCAC-60 cathode shows a small shift in the peak position with almost negligible change in peak current. The appearance of pronounced and well distinguished peak at 2.38 V appears for SCAC-66 cathode also, which is not significant as that of SCAC-60.The appearance of an additional anodic peak at 2.38 V observed during extended cycling is more pronounced in SCAC-60 cathode, compared with that of SCAC-66 cathode. Such an appearance of additional peak arises, when the sulfur forms an intimate contact with the carbon aerogel.[11] So, an overall improved performance has been observed for SCAC-60 cathode due to the availability of desired quantity of unfilled pores to buffer the volume expansion. The thermal distribution of sulfur in CA scaffold is found to get electrochemically redistributed, which reduces the polarization in oxidation peaks. The background current of CV curve shows the absence of unwanted red-ox reactions in the system, which is noteworthy.

The overall cycling performance observed in CV could be best understood and correlated using the following equations.

$$2Li + S \leftrightarrow Li_2S \text{ (overall reaction)} \quad (1)$$
$$2Li + S_8 \leftrightarrow Li_2S_8 \quad (2)$$
$$2Li + Li_2S_8 \leftrightarrow 2Li_2S_4 \quad (3)$$
$$2Li + Li_2S_4 \leftrightarrow 2Li_2S_2 \text{ (insoluble)} \quad (4)$$
$$2Li + Li_2S_2 \leftrightarrow 2Li_2S \text{ (insoluble)} \quad (5)$$

In short, reactions (2)-(3) correspond to the first plateau and the last two reactions to the second plateau.[38]

Electrochemical performance of different concentration of sulfur loaded CA cathodes has been evaluated using galvanostatic charge/discharge studies performed at C/10 rate (C=1675 mA/g_{sulfur}) (Fig. 9) and the current calculation has been made, based on the weight of sulfur in the electrode. Typical two plateau electrochemical reduction behavior of voltage profile has been exhibited by all the SCAC-X electrodes (Fig. 9(a)), thus evidencing the involvement of same reduction mechanism in all the chosen cathode formulations. Reduction begins from OCV, which ranges from 2.44 to 2.30 V and exhibits the presence of first and second reduction plateau, found to present closer to each other. This is an indication that more sulfur is physically adsorbed (free S_8).[24] The significant reduction of lower order polysulphides in the potential range below 2.1 V could be observed for SCAC-40 and 50 cathodes, due to the dissolution of higher amount of sulfur in the electrolyte. Single plateau oxidation occurs during the initial charging of all the cathodes. However, reasons such as higher electrolyte contact area on lower loading and the non availability of sufficient pores to buffer volume changes on more loading of sulfur are believed to be the reasons for the appearance of second oxidation plateau that has been observed for all the cathodes, with an exception of 60 wt. % loading (in 50^{th} cycle). Further, the length of the second plateau corresponds to 32- 37 % of the total charging capacity of the

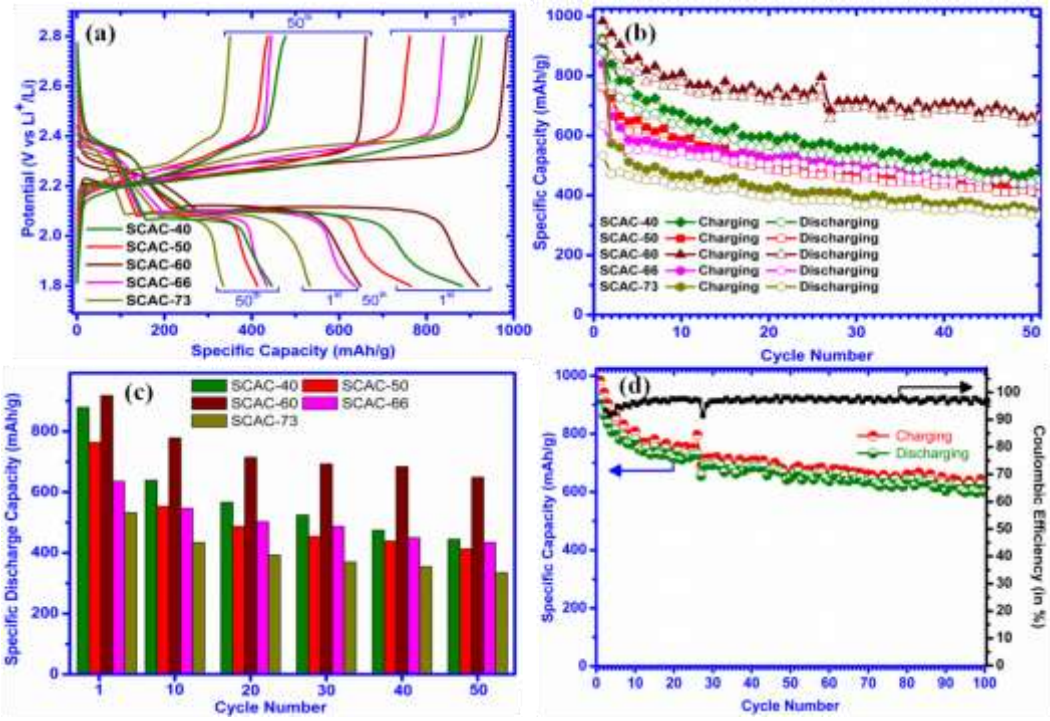

Fig. 9 (a) Comparative galvanostatic charge/discharge (b) cycle life (c) selective cycle life behavior of all sulfur-loaded carbon aerogel composites under a current rate of C/10 and (d) extended cycle life study of SCAC-60 cathode

individual cathodes, which is an indication that the resultant capacity arises from the reduction of higher order polysulfide to elemental sulfur. In other words, dissolved polysulfides (liquid state) are converted into solid sulfur, which gets accumulated on the surface of carbon rather than accommodating the pores of CA. The lesser polarization behavior exhibited by SCAC-60 composite cathode substantiates the recommendation of the same as the optimum composition of SCAC-X cathode, suitable for Li-S system. Further, the absence of second plateau observed with the SCAC-60 cathode is an evidence that the loaded sulfur has occupied the available pores of CA and no undesirable accumulation of sulfur could be seen on the surface of CA to reduce the effective utilization of sulfur. As a result, SCAC-60 cathode with negligible polarization change has been concluded as the better performing cathode through the present study.

Cycleability studies presented in Fig. 9(b) display initial discharge capacity values of 879, 763, 918, 636 and 533 mAh/g with respect to SCAC-X cathodes where X= 40, 50, 60, 66 and 73 respectively. Among the chosen cathodes, the lowest capacity has been observed for SCAC-66 and 73 cathodes. It is found that the capacity gets stabilized invariably after 10 cycles and the capacity of SCAC-X (X-40, 50, 60, 66, and 73) cathodes after 50 cycles is found to be 450, 413, 649, 435 and 335 mAh/g, which is about 51, 54, 71, 68, 63 % of the respecti ve initial capacity value. An appreciable and higher capacity value of 649 mAh/g with a better retention behavior has been shown by SCAC-60 cathode, as evident from Fig. 9(c). Based on these observations, SCAC-60 cathode has been subjected

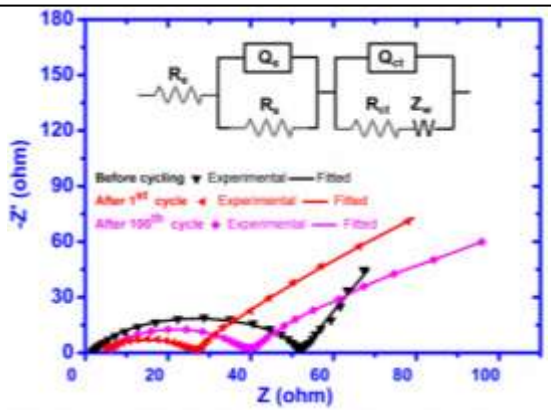

Fig. 10 Experimental and fitted Impedance spectra of the as fabricated cell containing SCAC-60 cathode and the cell after completing 1 and 100 cycles (Inset- corresponding equivalent circuit).

State	R_e (Ω)	R_{ct} (Ω)
Before cycling	**1.68**	**50.86**
After 1st cycling	**2.93**	**23.27**
After 100th cycling	**5.61**	**33.25**

Table 3 EIS parameters of SCAC-60 cathode at different state of cycling.

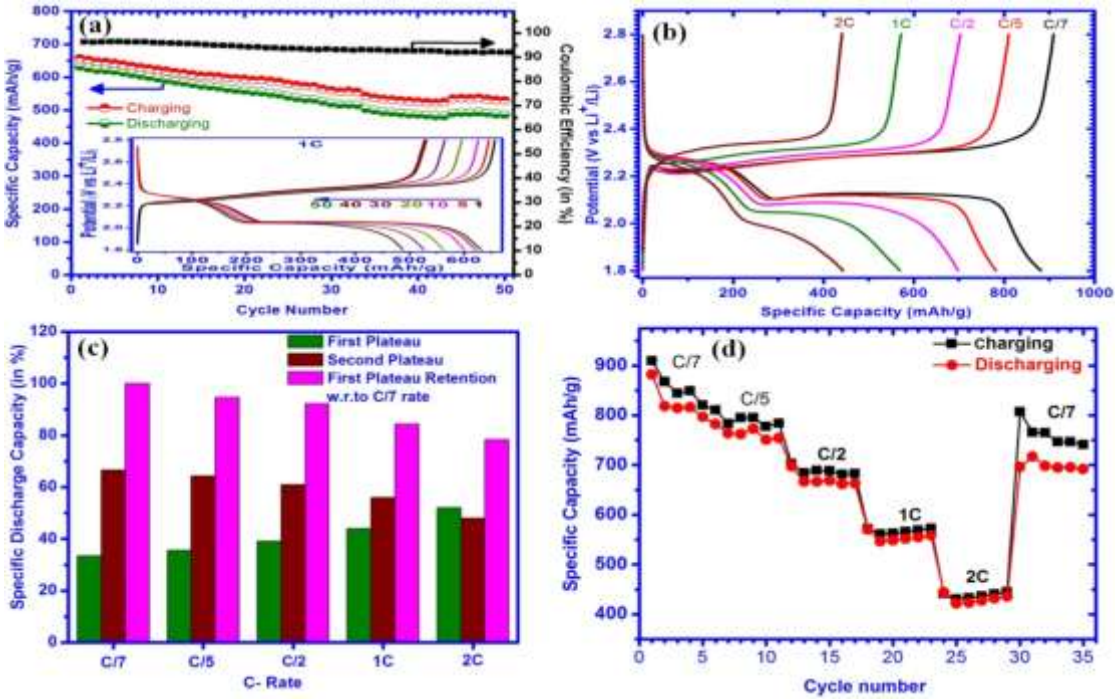

Fig. 11 (a) High (1C) rate cycling behavior (inset- selective discharge/charge curves) (b) discharge/charge curves (c) retention of discharge plateaus and (d) cycling and retention behavior of SCAC-60 cathode under the influence of different current rates.

further to extended cycleability, high rate performance and rate capability analyses.

Extended cycleability of SCAC-60 cathode (in Fig. 9(d)) at C/10 rate shows a nominal capacity of 600 mAh/g after 100 cycles with an acceptable degradation of 0.37 % per cycle. At the 100th cycle, it exhibits a capacity of 600 mAh/g, which is 87 % of 30th cycle and 93 % of 50th cycle capacity. Similarly, the coloumbic efficiency is found to be 90-95 % during the first 10 cycles and increased subsequently to 97 % upon extended cycling, due to improved stability.

Experimentally observed and fitted impedance spectra of the as fabricated cell containing SCAC-60 cathode and the cell after completing 1 and 100 cycles are furnished in Fig. 10 with an inset containing the corresponding equivalent circuit model. Closer resemblance of observed and calculated values is evident from the figure (Fig. 10). The fitted equivalent circuit contains various circuit elements such as R_e, $Q_s//R_s$, $Q_{ct}//R_{ct}$ and Z_W. Here, R_e is the electrolyte resistance, R_s is the surface resistance of lithium and SCAC-60 electrode, R_{ct} is the charge transfer resistance, Q_s and Q_{ct} are the constant phase elements and Z_W is the Warburg impedance[39]. From Table 3, the smaller R_e value of 1.68 Ω that has been observed before cycling exhibits small variation in electrolyte resistance even after completing 100 cycles. Such an observation indicates that cycling has not much altered the R_e of the cell and the small changes observed with respect to the R_e of the cell before and after cycling is believed to be due to the small amount of dissolution of loosely bound sulfur at CA. Depressed semicircle at higher-middle frequency range relates to the R_{ct} value of the cell and it shows 50.86 Ω before cycling, which is found to decrease to the extent of 23.27 and 33.25 Ω after 1st and 100th cycle respectively. As discussed in CV, the decrease in the charge transfer resistance after cycling is most likely due to the fact that sulfur gets rearranged in the pores and facilitates easy access to both electron and lithium ions. The slight increase in the charge transfer resistance indicates the superior conductive and buffering nature of CA to improve the electrochemical performance of sulfur. The observed inclined line in lower frequency region corresponds to the diffusion kinetics of electrode, which also follows the same trend for both 1st and 100th cycle. Hence, the lowest charge transfer resistance of the cell and the same trend observed in lower frequency region are due to the electrochemically favorable interface properties of CA with the electrolyte.

The role of CA as a conductive matrix to improve the performance of sulfur, formation of Li_2S and the related polysulfide retention in SCAC-60 cathode has been investigated under a high rated current of 1C, which is shown in Fig. 11(a). It demonstrates an initial capacity of 632 mAh/g with a coloumbic efficiency of 96 % and retention of 480 mAh/g at the 50th cycle, which is about 76 % of initial capacity and 86 % of 25th cycle capacity with a coloumbic efficiency of 92 %. This reveals the advantage of CA skeleton in improving the electrochemical behavior of sulfur even at high current rates and it emphasizes the polysulfide confinement at 1C rate. Hence, CA prepared in the current study offers multifarious benefits such as conducting additive, potential host for higher sulfur loading and better polysulfide confining matrix, which is

superior than the S@C composite, wherein carbon acts as a conducting additive only.[40]

The voltage profile of SCAC-60 cathode under the influence of different current rates, viz., C/7, C/5, C/2, 1C and 2C has been displayed in Fig. 11(b). While the polarization calculated against 50 % of the individual capacity is found to be small (155 mV) and similar for C/7 and C/5 rates, it is found to increase slightly (320 mV) for 2C rate. Such smaller polarization changes demonstrate the intimate contact of the sulfur with CA. However, part of the discharge capacity at 2C is limited by lower cut-off voltage, which is unavoidable. Even though SCAC-60 cathode provides a significant capacity of 422 mAh/g under the influence of 2C rate, the capacity limiting region in the discharge curve can be identified by evaluating the contribution of each region to the total capacity and the corresponding plot is given in Fig. 11(c). Contribution of first region on discharge curve (corresponds to conversion of S_8 to Li_2S_6) to the total capacity is 33, 36, 39, 44 and 52% for C/7, C/5, C/2, 1C and 2C rates respectively and the capacity retention of this region with respect to C/7 rate are 95, 92, 84, and 78% for C/5, C/2, 1C and 2C rates respectively. Capacity is mostly limited by the slow reduction kinetics of the second region.[41] Rate capability of the SCAC-60 cathode was evaluated under C/7 rate for first five cycles and subsequently at C/5, C/2, 1C, 2C rates for every other six cycles. Finally, the cell at 2C rate was brought back to C/7 discharge condition to understand the capacity retention behavior. From the rate capability study in Fig. 11(d), capacity values of 882, 782, 667, 547, 422 have been obsereved corresponding to C/7, C/5, C/2, 1C and 2C rates and finally the capacity gets resumed to 698 mAh/g for a rate of C/7. The three dimensional interconnected network of carbon aerogel with an ability to occupy ~70 wt. % sulfur shows a reversible capacity of 422 mAh/g at 2C rate up to six cycles and exhibits 698 mAh/g of capacity, when the current is switched back to C/7 rate for 60 wt. % sulfur loading.

The capacity obtained through the currently prepared sulfur-carbon aerogel composites is appreciable and superior than many other recent works. Y.Zhang et.al,[42] reported that nano-sulfur/polypyrrole/graphene composite with a loading of 52 wt. % exhibits a discharge capacity of 324.7 mAh/g at 50th cycle for 1C rate, which is 150 mAh/g lesser than this work and M.Agrawal et.al,[43] reported that porous carbon obtained through template method shows a discharge capacity of 400 mAh/g at 50th cycle for C/10 rate, which is 200 mAh/g lesser than the current work, especially with respect to the 100th cycle.

4. Conclusions

Carbon aerogel derived through an acid catalysed sol-gel polymerization of resorcinol-formaldehyde acts a potential host to accommodate ~70 wt. % of α-sulfur in the available pores. Interestingly, an increasing sulfur loading to the extent of 73 wt. %, results in the formation of monoclinic phase. A combination of amorphous and graphitic nature of CA offers synergistic advantages that include better buffering option against volume expansion and enhanced conductivity for the intermediately formed polysulfides along with those of Li_2S/Li_2S_2 and Li_2S_8 respectively. Among the selected S@C composites, SCAC-60 cathode exhibits an appreciable and progressive capacity of 600 mAh/g upto 100 cycles, with a capacity retention of 71 %. Further, an acceptable capacity of 480 mAh/g at 1C and 422 mAh/g at 2C rate has been exhibited by SCAC-60 cathode with an excellent coulombic efficiency of > 95 %. The carbon aerogel can house the reversible disproportional reaction of sulfur and lithium and offers favourable electrode-electrolyte interface for cycling, as understood from EIS measurements.

Acknowledgements

One of the authors K. Balakumar gratefully acknowledges Department of Science and Technology, India for offering INSPIRE fellowship (Code. No: IF120555). We acknowledge financial support of CSIR through MULTIFUN project (CSC-0101), Dr. N Lakshminarasimhan for BET analysis and Mr. Gopala Ram Bhadu and Dr. Divesh N. Srivastava for HRTEM and STEM analyses.

Notes

Electrochemical Power System Division, CSIR-Central ElectroChemical Research Institute, Karaikudi- 630 006, India. E-mail: kalaiselvicecri @gmail.com

References

1 P. G. Bruce, B. Scrosati and J. M. Tarascon, *Angew. Chem. Int. Ed. Engl.*, 2008, **47**, 2930–2946.
2 B. Kang and G. Ceder, *Nature Letters*, 2009, **458**, 190-193.
3 X. P. Xue-Ping Gao and H. X. Yang, *Energy Environ. Sci.*, 2010, **3**, 174–189.
4 B. Scrosati, J. Hassoun and Y. K. Sun, *Energy Environ. Sci.*, 2011, **4**, 3287- 3295.
5 Y. Wang, Z. S. Feng, J. J. Chen, C. Zhang, X. Jin and J. Hu, *Solid State Commun.*, 2012, **152**, 1577–1580
6 P. G. Bruce, S. A. Freunberger, L. J. Hardwick and J. M. Tarascon N*at. Mater*., 2012, **11**, 19-29.
7 D. Marmorstein, T. H. Yu, K. A. Striebel, F. R. Mclarnon, J. Hou and E. J. Cairns, *J. Power Sources*, 2000, **89**, 219-26.
8 Y. V. Mikhaylik and J. R. Akridge, *J. Electrochem. Soc.*, 2004, **151**, A1969- A1976.
9 X. He, J. Ren, L. Wang, W. Pu, C. Jiang and C. Wan, *J. Power Sources*, 2009, **190**, 154-156.
10 C. Liang, J. N. Dudney and J. Y. Howe, *Chem. Mater*., 2009, **21**, 4724–4730.
11 X. Ji, K. T. Lee and L. F. Nazar, *Nat. Mater*., 2009, **8**, 500-506.
12 N. Jayaprakash, J. Shen, S. S. Moganty, A. Corona and L. A. Archer, *Angew. Chem. Int. Ed.*, 2011, **50**, 5904-5908.
13 G. Zheng, Y. Yang, J. J. Cha, S. S. Hong and Y. Cui, *Nano Lett.*, 2011, **11**, 4462-4467.
14 J. Guo, Y. Xu and C. Wang, *Nano Lett.*, 2011, **11**, 4288-4294.
15 J. Z. Wang, L. Lu, M. Choucair, J. A. Stride, X. Xu and H. K. Liu, *J. Power Sources*, 2011, **196**, 7030-7034.

16 H. Wang, Y. Yang, Y. Liang, J. T. Robinson, Y. Li, A. Jackson, Y. Cui and H. Dai, *Nano Lett.*, 2011, **11**, 2644-2647.
17 A. K. Geim and K. S. Novoselov, *Nat. Mater.*, 2007, **6**, 183-191.
18 Y. Wang, Z. S. Feng, C. Zhang, L. Yu, J. J. Chen, J. Hua and X. Z. Liu, *Nanoscale*, 2013, **5**, 3704-3712.
19 X. Liang, Y. Liu, Z. Wen, L. Huang, X. Wang and H. Zhang, *J. Power Sources*, 2011, **196**, 6951-6955.
20 F. Wu, J. Chen, R. Chen, S. Wu, L. Li, S. Chen and T. Zhao, *J. Phys. Chem. C*, 2011, **115**, 6057-6063.
21 H. Chen, W. Dong, J. Ge, C. Wang, X. Wu, W. Lu and L. Chen, S*ci. Rep.*, DOI: 10.1038/srep01910.
22 S. C. Zhang, L. Zhang, W. K. Wang and W. J. Xue, *Synth. Met.*, 2010, **160**, 2041-2044.
23 J. Wang, J. Yang, J. Xie and N. Xu, *Adv. Mater.*, 2002, **14**, 963-965.
24 X. Ji, S. Evers, R. Black and L. F. Nazar, *Nat. Commun.*, DOI: 10.1038/ncomms 1293.
25 Y. J. Choi, B. S. Jung, D. J. Lee, J. H. Jeong, K. W. Kim, H. J. Ahn, K. K. Cho and H. B. Gu, *Phys. Scr.*, 2007, **T129**, 62-65.
26 C. Lin and J. A. Ritter, *Carbon*, 1997, **35**, 1271-1278.
27 R. W. Pekala, *J. Mater. Sci.*, 1989, **24**, 3221-3227.
28 J. Gao and H. D. Abruna, *J. Phys. Chem. Lett.*, 2014, **5**, 882-885.
29 Z. Zhang, Z. Li, F. Hao, X. Wang, Q. Li, Y. Qi, R. Fan and L. Yin, *Adv. Funct. Mater.*, 2014, **24**, 2500-2509.
30 S. Moon, Y. H. Jung, W. K. Jung, D. S. Jung, J. W. Choi and D. K. Kim, *Adv. Mater.*, 2013, **25**, 6547–6553.
31 R. J. Nemanich and S. A. Solin, *Phys. Rev. B*, 1979, **20**, 392-401.
32 A. T. Ward, *J. Phys. Chem.*, 1968, **72**, 744-746.
33 T. Horikawa, D. D. Do and D. Nicholson, *Adv. Colloid. Interface Sci.*, 2011, **169**, 40-58.
34 H. Ago, T. Kugler, F. Cacialli, W. R. Salaneck, M. S. P. Shaffer, A. H. Windle and R. H. Friend, *J. Phys. Chem. B*, 1999, **103**, 8116-8122.
35 B. Guo, T. Ben, Z. Bi, G. M. Veith, X. G. Sun, S. Qiu and S. Dai, *Chem. Commun.*, 2013, **49**, 4905-4907.
36 M. S. Park, J. S. Yu, K. J. Kim, G. Jeong, J. H. Kim, Y. N. Jo, U. Hwang, S. Kang, T. Woo and Y. J. Kim, *Phys. Chem. Chem. Phys.*, 2012, **14**, 6796-6804.
37 Y. X. Wang, L. Huang, L. C. Sun, S. Y. Xie, G. L. Xu, S. R. Chen, Y. F. Xu, J. T. Li, S. L. Chou, S. X. Douc and S. G. Sun, J. Mater. Chem., 2012, 22, 4744-4750.
38 S. S. Jeong, Y. T. Lim, Y. J. Choi, G. B. Cho, K. W. Kim, H. J. Ahn, and K. K. Cho, *J. Power Sources*, 2007, **174**, 745-750.
39 M. Hagen, G. Feisthammel, P. Fanz, H. T. Grossmann, S. Dorfler, J. T¨ubke, M. J. Hoffmann, D. Borner, M. Joos, H. Althues, and S. Kaskel, *J. Electrochem. Soc.*, 2013, **160**, A996-A1002.
40 H. S. Ryu, Z. Guo, H. J. Ahn, G. B. Cho and H. Liu, *J. Power Sources*, 2009, **189**, 1179-1183.
41 H. Yamin, A. Gorenshtein, J. Penciner, Y. Sternberg and E. Peled. *J. Electrochem. Soc.*, 1988, **135**, 1045-1048.
42 Y. Zhang, Y. Zhao, A. Konarov, D. Gosselink, H. G. Soboleski and P. Chen, *J. Power Sources*, 2013, **241**, 517-521.
43 M. Agrawal, S. Choudhury, K. Gruber, F. Simon, D. Fischer, V. Albrecht, M. Gobel, S. Koller, M. Stamm and L. Ionov, *J. Power Sources*, 2014, **261**, 363-370.